Volume 4
Number 2
February 2025
Pages 183–328

Environmental Science Advances

rsc.li/esadvances

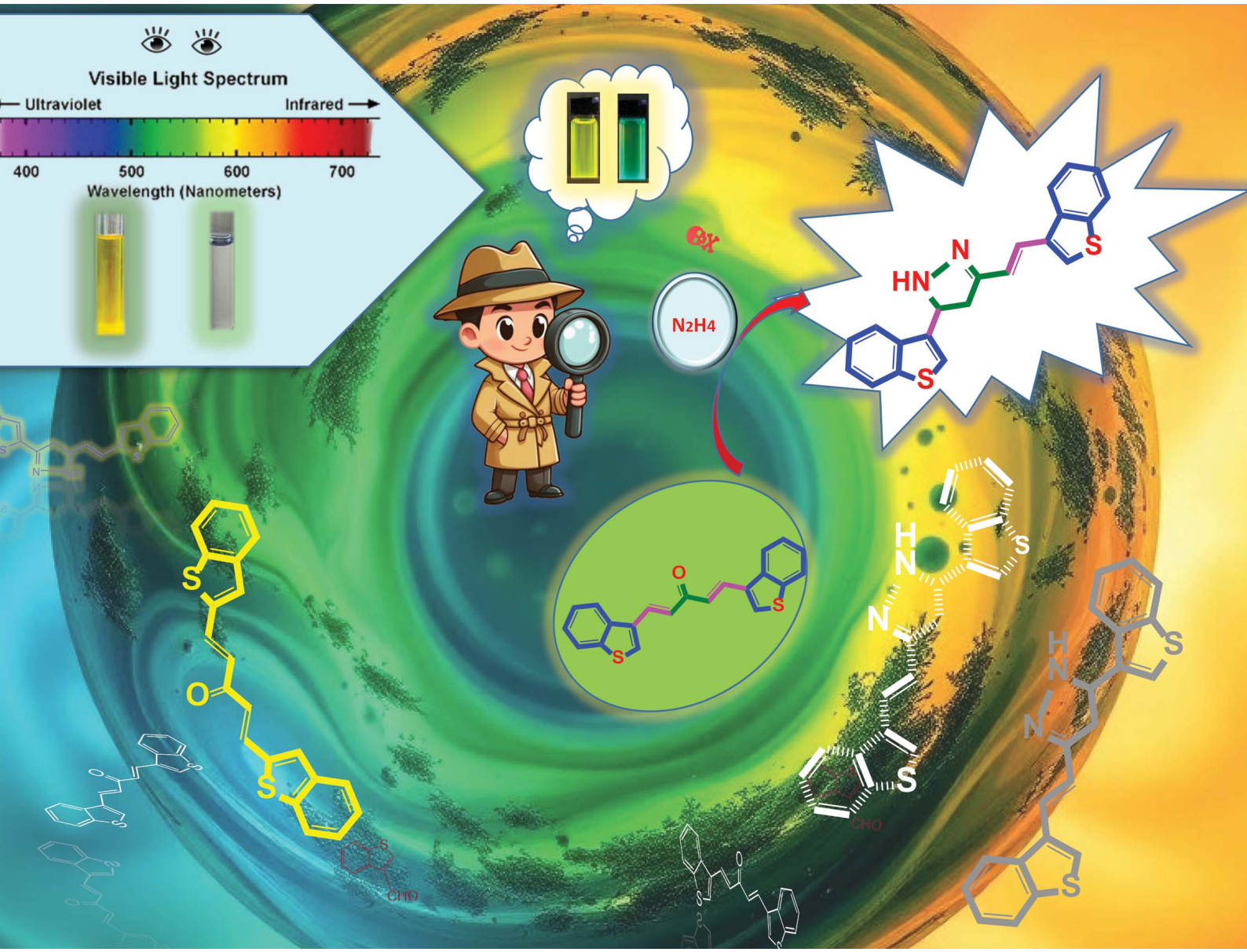

ISSN 2754-7000

ROYAL SOCIETY OF CHEMISTRY

PAPER

Paresh N. Patel *et al.*

Benzothiophene based semi-bis-chalcone as a photo-luminescent chemosensor with real-time hydrazine sensing and DFT studies

Environmental Science Advances

ROYAL SOCIETY OF CHEMISTRY

PAPER

View Article Online
View Journal | View Issue

Cite this: *Environ. Sci.: Adv.*, 2025, **4**, 235

Benzothiophene based semi-bis-chalcone as a photo-luminescent chemosensor with real-time hydrazine sensing and DFT studies†

Nidhi H. Oza, Dinkal Kasundra, Amar G. Deshmukh, Niteen Borane, Rajamouli Boddula and Paresh N. Patel *

Hydrazine is a very toxic chemical that poses a major threat to human health and the environment. As a further expansion of our ongoing research, this report validates the enhanced real-time hydrazine sensing using benzothiophene-based semi-bis-chalcone (SBC). Hypothesized SBC molecules that can be easily attacked by nucleophilic groups were synthesised *via* classical Claisen–Schmidt condensation. Two derivatives of novel SBC scaffolds were synthesised by the reaction of simple acetone with benzothiophene carbaldehydes. This reaction involved the use of KOH and pyrrolidine as catalysts, and they demonstrated two different processes in comparative studies. KOH worked as a speedy catalyst, while pyrrolidine was demonstrated to be a more efficient catalyst. The structures of the synthesised compounds were established by various spectral techniques. The optical properties of the prepared SBCs were studied in different solvent systems and demonstrated that methanol was the more suitable solvent. Density functional theory (DFT) calculations of both compounds in methanol were performed using the Gaussian software. Time-dependent density functional theory (TDDFT) calculations were performed to study the dynamic behaviour of electrons in both molecules and materials by considering their density as a function of time. Both DFT and TDDFT calculations were observed to have a good correlation with the experimental results. The obtained absorption and photoluminescence results and their theoretical correlation suggested that the prepared SBCs can be optimized for applications in optoelectronics, sensing, and bioimaging. As an improvement to our earlier protocol, more efficient real-time hydrazine sensing SBCs probes were established with prolonged π-conjugation. An exhaustive protocol with a working pH range, analyte selectivity, and real sample test was developed. The studied SBCs showed a broad working pH range and excellent hydrazine sensing selectivity. With these two included in our large library of photoresponsive molecules, we aim to construct a model device for hydrazine sensing in real life applications.

Received 3rd August 2024
Accepted 29th October 2024

DOI: 10.1039/d4va00306c

rsc.li/esadvances

Environmental significance

As per the journal scope, the present study highlights the synthesis of highly conjugated novel hetero-aryl substituted semi-bis-chalcone (SBC) scaffolds of the benzothiophene moiety. Structures of the prepared molecules were determined using various spectral techniques. As per our knowledge, this is the first report on a hetero-aryl substituted semi-bis-chalcone (SBC) of acetone. The photophysical properties of these conjugated scaffolds were investigated by dual spectroscopic techniques. They exhibited very effective photo-luminescent properties. DFT calculations of both compounds in methanol were performed using Gaussian software. TDDFT calculations were performed to study the dynamic behaviour of electrons in both molecules by considering their density as a function of time. The obtained results from all these studies suggested that the prepared SBCs can be optimized for their applications in optoelectronics, sensing, and bio-imaging. Therefore, these molecules were investigated for hydrazine sensing studies. Various solvent screening and titrations with different hydrazine concentrations were performed. The competitive selectivity of the prepared probe to different analytes and the pH dependence were also studied. A mechanistic study of the sensing reaction was also performed. These results prove that, compared to our earlier reports and other literature, these SBCs are highly selective and efficient sensors for hydrazine.

1 Introduction

Hydrazine has considerable industrial uses due to its strong alkalinity, nucleophilicity and high reducing power.[1] It has been used to produce pesticides, drugs, pharmaceutical intermediates, catalysts, textile dyes, plastic polymers, anti-hypertensive

Laboratory of Bio-Organic Chemistry, Tarsadia Institute of Chemical Science (TICS), Uka Tarsadia University, Bardoli 394 350, Gujarat, India. E-mail: pareshn111@yahoo.com

† Electronic supplementary information (ESI) available. See DOI: https://doi.org/10.1039/d4va00306c

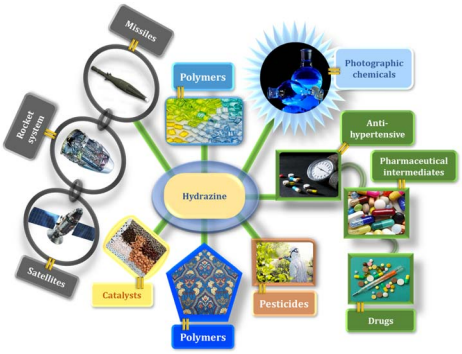

Fig. 1 Hydrazine-diversified multipurpose applications.

hydralazine and photographic compounds.[2,3] Additionally, it has been used as a high-energy fuel propellant for rocket propulsion systems, missiles and satellites (Fig. 1).[4–6]

However, one deadly consequence of hydrazine is environmental pollution.[7,8] The effects of hydrazine on biological systems and numerous biochemical processes at the cellular level are also a major concern.[9] Excessive exposure to this highly hazardous substance can cause skin irritation and damage to the liver, kidney, and central nervous system.[10] As a result, its negative impacts create safety issues for its widespread usage in bulk production, transport and waste water disposal operations, which might result in major environmental contamination. The US Environmental Protection Agency (EPA) has since classified it as a potential carcinogen to living organisms and has advised a low threshold limit value (TLV) of 10 ppb hydrazine in drinking water.[11,12]

As a result, there has been a pressing need to develop efficient, sensitive and selective probes for monitoring hydrazine-contaminated environments. So far, hydrazine has been identified and quantified using a range of traditional techniques.[13–15] In the last few years, numerous strategies have been established to sense hydrazine, including gas and high-performance liquid chromatography,[16,17] atomic absorption spectroscopy,[18] colorimetric[19] and electrochemical analysis.[20] These techniques all have significant inadequacies, such as awkward operation, complex sample preparation and the huge quantities of samples required. Due to its on-site detection and relevance to biological and environmental applications, spectroscopic determinations are more common and favoured among these approaches.[21] However, to improve the operational convenience, cost-effectiveness, quick detection and high selectivity at low ppm level, efforts have been made in recent years to create novel fluorescent sensors.[21–23]

Fluorescent sensors are a modern analytic tool with better reliability, simplicity, operability and low-cost, among other advantages.[24–26] Some of the most recent fluorescent sensors for hydrazine detection are based on three different reaction mechanisms: (i) hydrazine-assisted cleavage of protecting groups of levulinoyl ester or acetyl groups, 4-bromobutyrate; (ii) selective reaction with vinyl maleonitrile, barbituric acid; and (iii) hydrazine addition on an unsaturated system.[27–30] Although a large number of hydrazine fluorescent sensors have been

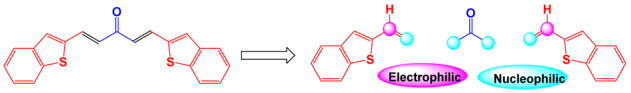

Scheme 1 Bis-[2 + 1] condensation to synthesize SBCs.

established,[31–35] these methods usually limit their applicability due to their low selectivity, sensitivity, limited pH range, specific temperature, long detection period, as well as multistep synthesis. As a result, there is a need to develop simple fluorescent probes for the detection of hydrazine that will overcome all these limitations from the previously reported probes.[36–40]

Herein, we report a one-step design strategy for the building of benzothiophene-treated SBCs as ratio-metric fluorescent sensors, which can detect hydrazine efficiently in real sample analysis. We have demonstrated two comparative methods catalysed by the cost-effective organic base pyrrolidine and inorganic base KOH. This hypothesized [2 + 3] Claisen–Schmidt condensation can be performed at room temperature (Scheme 1).

It starts *via* amphiphilic (*i.e.*, 1C, 2C) acetone having a nucleophilic methyl carbon and an electrophilic carbonyl carbon. It follows the five-carbon-centre condensation with an electrophilic aldehyde (*i.e.*, 1O, 3C) to form SBCs. The resultant product with a strong photoluminescent nature is used to develop an effective technique for the selective detection of hydrazine, and the results are presented here. These sensors are capable of providing the real time determination of hydrazine levels in the environment. The mechanistic investigation for the hydrazine detection study is also proven by spectral analysis and presented here.

2 Experiments

2.1 Synthesis of SBCs from benzothiophene aldehydes[41]

Benzothiophene aldehydes (**1a**/**1b**; 10 mmol) were dissolved in the least amount of ethanol (3 mL) as a solvent, and stirred to form a homogenous mixture in 10 mL RBF. Acetone (2; 5 mmol) was added dropwise to the stirred solution, and the resultant mixture was continually stirred at room temperature for 5 minutes. Later, a catalytic quantity of KOH or pyrrolidine solution in ethanol (4%, 2 mL) was added dropwise (Scheme 2). Finally, the resultant reaction mixture was stirred at room temperature for 1–2 h (for KOH)/3–4 h (for pyrrolidine). The completion of the reaction was monitored by thin layer chromatography (TLC) using ethyl acetate/*n*-hexane (1 : 3 v/v) as a solvent system. The product began to precipitate out in the reaction mixture as the reaction continued. After completion of the reaction, the precipitated product (**3a**/**3b**) was cooled and collected by filtration. The obtained residues were washed with cold ethanol, and purified by recrystallization through chloroform–methanol (2 : 1 v/v, 8 mL).

2.2 Photophysical properties of SBCs and their hydrazine detection study

The photophysical properties of both prepared SBCs were investigated by UV-visible absorption and fluorescence

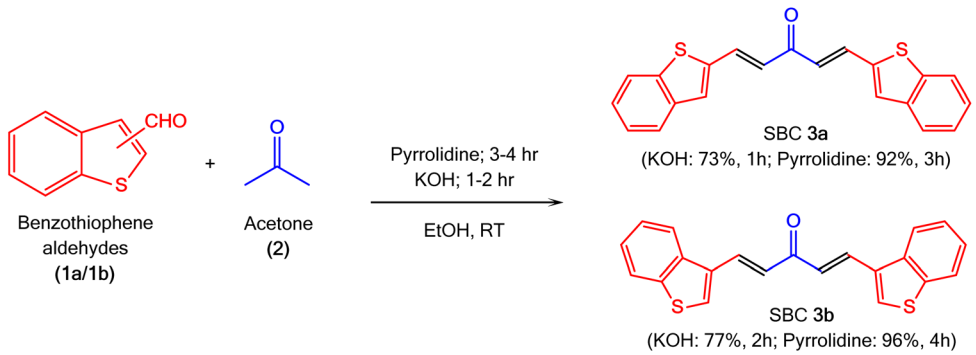

Scheme 2 Synthetic root for SBCs formation from benzothiophene aldehydes.

emission experiments using their 5 μM solution. To find the more appropriate solvent for the UV-visible absorption and fluorescence emission experiments, the solvents were screened with the same concentration in different HPLC grade solvents. Based on the Stokes shift values of both SBCs in different solvents, methanol was chosen for absorption-emission titrations of the hydrazine detection study with a fixed concentration of SBCs (5 μM) and varied concentration of hydrazine in methanol (0–8 μM). The operational solutions with different concentrations (2–8 μM) of hydrazine for detection studies were made by serial dilution in HPLC grade methanol.

3 Results and discussion

3.1 Synthesis of novel SBCs derivatives

Two novel Semi-Bis-Chalcone molecules (**3a**/**3b**) were synthesized by Claisen–Schmidt condensation of acetone (**2**) and benzothiophene aldehydes (**1a**/**1b**) in EtOH at room temperature (Scheme 2). These derivatives were synthesized with two separate catalysts, *i.e.*, pyrrolidine and KOH, to evaluate their influence on the product isolated yield and reaction time. These experimental results have clearly shown that pyrrolidine is an efficient substitute of KOH. The reactions were completed in a shorter reaction time for the KOH-catalysed experiments. However, there were significantly lower yields compared to the pyrrolidine-catalysed experiments. The lower isolated yield could be because of the significant solubility of the obtained chalcone in ethanolic KOH. These results show that pyrrolidine is an efficient catalyst for the reaction under milder conditions with a higher isolated yield in an extended reaction time. The prolonged reaction time could be because of the weak basic nature of pyrrolidine.

3.2 Structure confirmation of the prepared SBC molecules by spectral studies

The structures of all of the newly prepared molecules were confirmed by different spectroscopic techniques, like NMR, IR and HRMS. All of the spectra and spectral data are given in the ESI.† In the ^{1}H NMR spectrum of SBC **3a**, two clear peaks as a doublet with a similar coupling constant of 15.5 Hz were observed at 7.965 and 6.905 δppm. These peaks confirmed the presence of two α and two β symmetric protons with *trans* geometry on the *bis*-α,β-unsaturated carbonyl system, respectively. One clearer singlet was observed at 7.574 δppm corresponding to two symmetric protons on the third position of the thiophene ring of the benzothiophene moieties. An additional two multiplets were observed at 7.794–7.841 and 7.386–7.417 δppm, corresponding to eight protons of the benzene ring of the benzothiophene moieties. The presence of the carbonyl group was further supported with the ^{13}C NMR spectrum by the peak observed at 187.46 δppm, along with twelve symmetric carbons in the aromatic region of 122.58–140.22 δppm. The structure of SBC **3a** was also confirmed by its HRMS spectrum. Here, the observed molecular weight (347.0716 gm per mole) perfectly matched with its calculated molecular weight (347.0712 gm per mole). The presence of a carbonyl group was additionally confirmed by FT-IR spectrum with a band at 1789 cm^{-1}, along with a C–S stretching mode at 825 cm^{-1}, aromatic C=C stretching mode at 1600 cm^{-1} and a C–H stretching at 3025 cm^{-1}. Similarly, the structure of SBC **3b** was also confirmed with ^{1}H NMR, ^{13}C NMR, HRMS and FT-IR spectral analyses.

3.3 Photophysical properties of the prepared SBCs

To study the hydrazine sensing ability of the synthesized novel Semi-Bis-Chalcone molecules, screening of both SBCs was performed. Based on the Stokes shift values of both SBCs in methanol (Table 1), SBC **3b** with the highest Stokes shift was chosen for the absorption-emission titrations of the hydrazine detection study. The most suitable solvent for this investigation was selected by studying the photophysical properties of SBC **3a** and **3b** in different solvents with varied polarity from hexane to water (Fig. 2A and S7†). The main absorption peak at ∼360 nm was observed in all absorption spectra of SBC **3b** in different solvents. Hexane and toluene, as less polar solvents, show the longer absorption peak (362 nm, $\varepsilon = 3.51 \times 10^{4}$ cm^{-1} M^{-1}). Conversely, methanol and DMSO as polar solvents show the shorter absorbance (340 nm, $\varepsilon = 2.25 \times 10^{4}$ cm^{-1} M^{-1}) of the SBC **3b**. The photophysical characteristics of SBC **3a** and **3b** in different solvents with varied polarity were also studied by fluorescence spectra (Fig. 2B and S7†). As seen in the normalized fluorescence spectra, the emission maxima of SBC **3b**

Table 1 Photophysical parameters of SBCs

	Solvent							
SBCs	Hexane	Toluene	ACN	THF	Acetone	Methanol	DMSO	Parameters
3a	352	366	351	357	349	370	344	λ_{abs} (nm)
	430	405	473	407	—	532	433	λ_{em} (nm)
	78	39	122	50	—	162	89	$\Delta\lambda$ (nm)
	3.37×10^4	4.50×10^4	2.78×10^4	3.02×10^4	1.29×10^4	3.17×10^4	2.08×10^4	ε (M^{-1} cm^{-1})
3b	362	370	349	355	352	368	340	λ_{abs} (nm)
	427	398	465	408	—	537	436	λ_{em} (nm)
	65	28	116	53	—	169	96	$\Delta\lambda$ (nm)
	3.51×10^4	4.60×10^4	2.92×10^4	3.18×10^4	1.57×10^4	3.52×10^4	2.25×10^4	ε (M^{-1} cm^{-1})

gradually varied with the change of the solvent polarity from hexane to water. The emission peak positions show an obvious red shift from 427 nm in hexane to 537 nm (methanol), as anticipated for the increase in solvent polarity. Methanol shows better UV absorption and fluorescence emission properties of SBC **3b** among all the studied solvents. Thus, all the hydrazine sensing studies were carried out in methanol (Fig. 3).

3.4 Hydrazine sensing study by 3b

To determine the hydrazine sensing range of SBC **3a** and **3b**, the titration of hydrazine with varied concentration (0 to 5 μM) *vs.* SBC **3a**/**3b** with fixed concentration (5 μM) was carried out *via* absorption and emission spectroscopy (Fig. 4a and S8†). The absorption maxima of SBC **3b** at 368 nm gradually decreased with increasing hydrazine concentration and a major blue shift (368 to 335 nm) in the absorption maxima was also observed. The color also changed from yellow to colorless (graphical abstract). This shows that SBC **3b** can be used as a sensor for hydrazine that can be observed by naked eye. The compound SBC **3b** shows fluorescence emission at 537 nm, which is similar to the bright blue fluorescence. After the increase of the hydrazine concentration, a quenching in the fluorescence emission at 537 nm ($\lambda_{ex} = 368$ nm) was observed. The detection limit of the studied molecule (5 μM) in terms of the minimum amount of hydrazine is 5 μM with 90% accuracy. Additionally, the fluorescence color before and after the titration changes from bright blue to almost zero emission. These titration experiments were accomplished within 2 minutes of each other, showing the sensitivity of the probe towards hydrazine. Overall, this investigation proves the efficacy of compound SBC **3b** for the exposure of hydrazine even at very low concentrations.

3.5 Interfering analytes of hydrazine sensing studies for SBC 3b

To check the discrimination and anti-interference of SBC **3b** for its actual application, a competitive study for the preference of SBC **3b** with other interfering chemicals was conducted. Initially, the emission studies at 537 nm were done with solutions of 5 μM SBC **3b** and 5 μM of various interfering chemicals. The obtained results clearly showed the negligible effect of the interfering chemicals on the emission property of SBC **3b** (Fig. 4, solid column). Later, 5 μM hydrazine was added to all of these solutions and the emission was studied at 537 nm. The observed results clearly showed very high quenching in the emission property of SBC **3b** in the presence of interfering chemicals (Fig. 4, dotted column). This study demonstrated SBC **3b** as an exceptional optical sensor for hydrazine with great selectivity and anti-interference in the presence of all of the studied interfering chemicals.

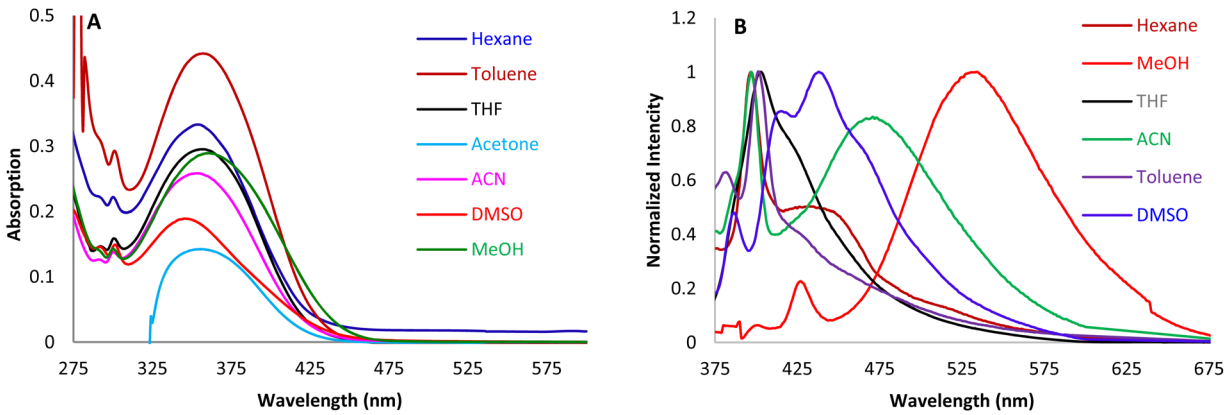

Fig. 2 (A) UV-vis absorption and (B) normalized fluorescence spectra of SBC **3b** (5 μM) in various solvents.

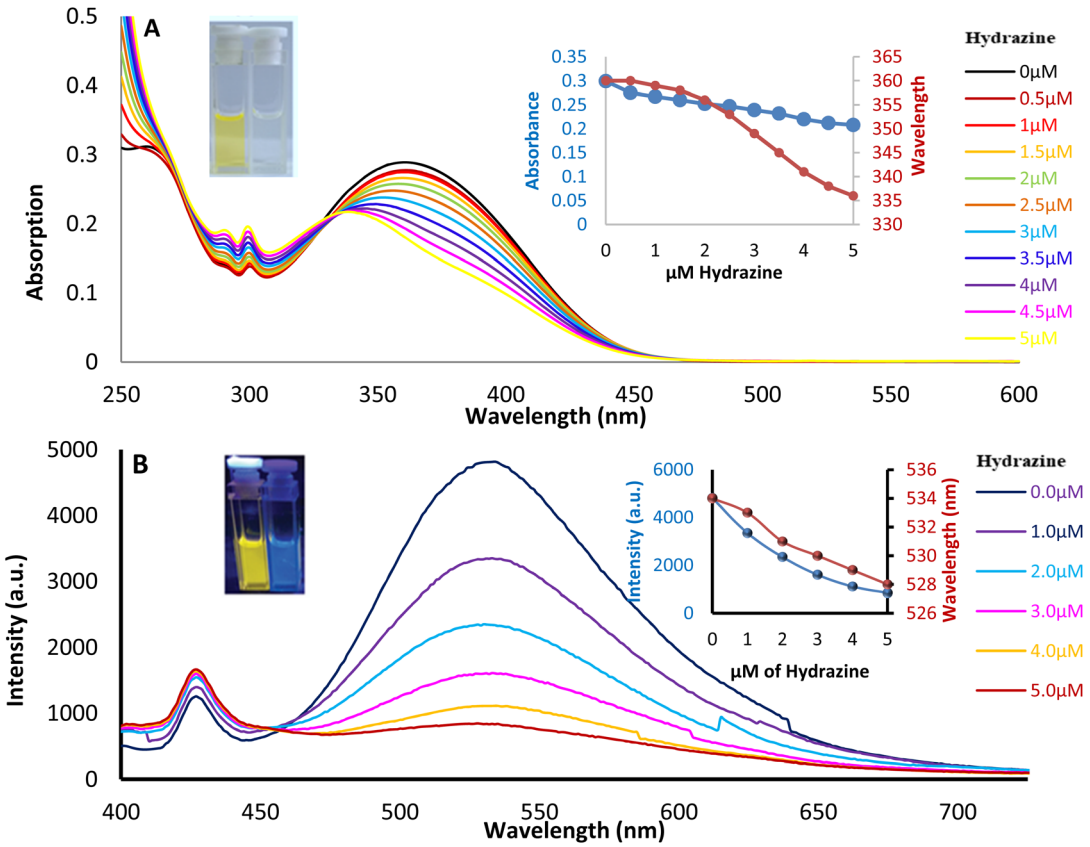

Fig. 3 Hydrazine (0.0 to 5.0 μM) *vs.* SBC **3b** (5.0 μM) titration by (A) UV-vis absorption and (B) fluorescence emission (λ_{ex} = 358 nm) studies in methanol.

3.6 Mechanistic exploration of the detection study by 3b

As per our earlier studies,[28–30] to find the mechanistic track (Scheme 3) for the sensing of hydrazine, the resultant mixture of **3b** and hydrazine in methanol after the emission study was injected into a GC-MS (Fig. S6†). The witnessed *m*/*z* value clearly ratified the formation of 1H-pyrazole (**3b-NH2NH2**). Similarly, it was also confirmed by NMR and FT-IR analysis, as discoursed in ESI.† The sensing mechanism possibly progressed through the unsteady intermediate imine formation by nucleophilic attachment on the carbonyl carbon, followed by dehydration.

3.7 Effect of pH on the SBC 3b emission

The pH value has a great influence on the chemosensing study. Therefore, a study involving the pH effect on the SBC **3b** (Fig. 5)

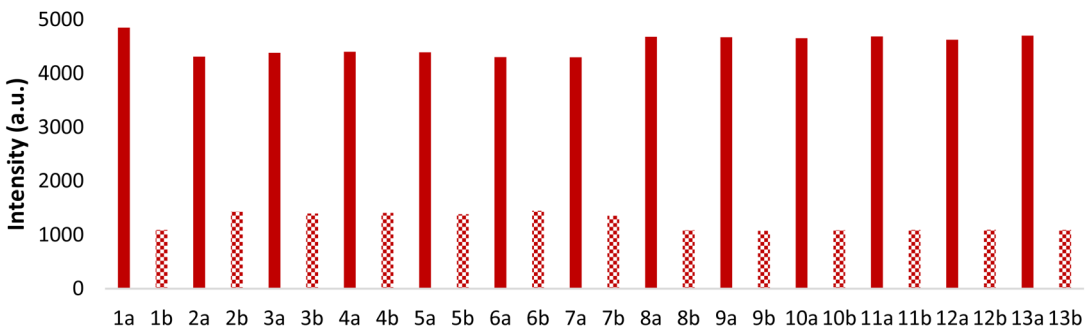

1a-3b, **1b**-3b + hydrazine, **2a**-3b + EDA, **2b**-3b + EDA + hydrazine, **3a**-3b + Urea, **3b**-3b + Urea + hydrazine, **4a**-3b + Propyl amine, **4b**-3b + Propyl amine + hydrazine, **5a**-3b + Ethyl amine, **5b**-3b + Ethyl amine + hydrazine, **6a**-3b + TEA, **6b**-3b +TEA + hydrazine, **7a**-3b + DEA, **7b**-3b + DEA + hydrazine, **8a**-3b + $NaNO_2$, **8b**-3b + $NaNO_2$ + hydrazine, **9a**-3b + $AgNO_3$, **9b**-3b + $AgNO_3$ + hydrazine, **10a**-3b + $CuCl_2{\cdot}2H_2O$, **10b**-3b + $CuCl_2{\cdot}2H_2O$ + hydrazine, **11a**-3b + $MgSO_4$, **11b**-3b + $MgSO_4$ + hydrazine, **12a**-3b + $ZnCl_2$, **12b**-3b + $ZnCl_2$ + hydrazine, **13a**-3b + $BaCl_2$, **13b**-3b + $BaCl_2$ + hydrazine

Fig. 4 Selectivity of SBC **3b** (5 μM; 537 nm) for hydrazine against different interfering analytes.

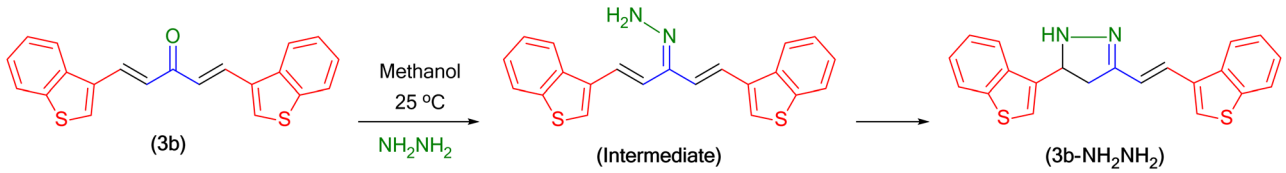

Scheme 3 The mechanistic path for the sensing of hydrazine by SBC **3b**.

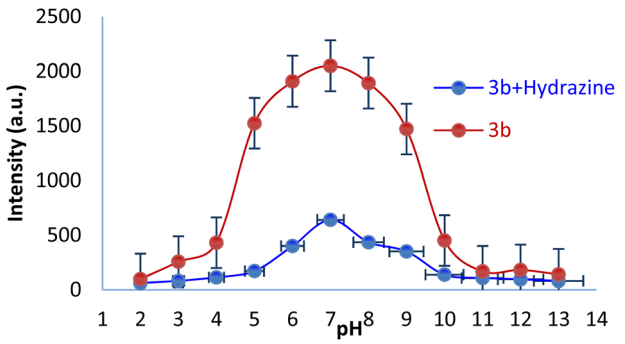

Fig. 5 Effect of pH on the hydrazine sensing study by SBC **3b** (5 μL; 537 nm).

emission property was executed to find out the working pH range for **3b**. The attained results confirmed that it has excellent sensing capability for hydrazine in the 5.0–10.0 pH range, which was observed in our earlier reports.[28–30]

3.8 The real time hydrazine sensing by SBC 3b in water and soil samples

The above studies show that **3b** may have reasonable sensing capability for hydrazine in real water and soil samples. Therefore, the use of SBC **3b** for sensing of hydrazine in various soils was also investigated.

As a part of the 1st investigation, 1 g of clay soil/field soil/sandy soil was added to SBC **3b** (5 μM) solution in methanol (5 mL). The fluorescence emission spectra of the supernatants were recorded (Fig. 6), which showed that there is no major influence from the different soil samples on the emission nature of **3b**. This observation has shown that the chemicals in the different soils did not affect the emission nature of **3b**. As a 2nd investigation, 1 g of clay soil/field soil/sandy soil was polluted with hydrazine (5 μM), and then it was added to the **3b** (5 μM) solution in methanol (5 mL). Once again, the fluorescence emission spectra of the supernatants were recorded, and it showed a large decrease in the emission signal of SBC **3b**.

Observing all these experiments with the quick reaction time, high sensing capacity, anti-interference and excellent selectivity of SBC **3b**, the sensing study of SBC **3b** on hydrazine in real water samples was also performed. Potable water is known to have some level of minerals and dissolved organic substances, including Na^+, Cu^{2+}, Mg^{2+}, Fe^{3+}, and ClO^-.

Therefore, SBC **3b** was lastly examined for hydrazine sensing in various samples of water, *i.e.*, tap water, river water and mineral water. Initially, the solution of SBC **3b** (0.5 μM) in methanol was mixed with all three different water samples and the emission spectra were recorded (Fig. 7). The attained results have evidently shown that these water samples have not influenced the emission nature of **3b**. A very low but substantial decrease in emission was present in the river water sample. This could be because of the presence of hydrazine or another similar analyte. However, after the addition of an equal amount of hydrazine (0.5 μM) in all of these water samples, there was a huge decrease in the emission intensity of SBC **3b**. This shows the competence of the hydrazine sensing process in real time sample analysis.

3.9 DFT and TDDFT calculation

The obtained experimental analysis was confirmed further *via* density functional theory. Their excited energy levels were calculated *via* time-dependent density functional theory.

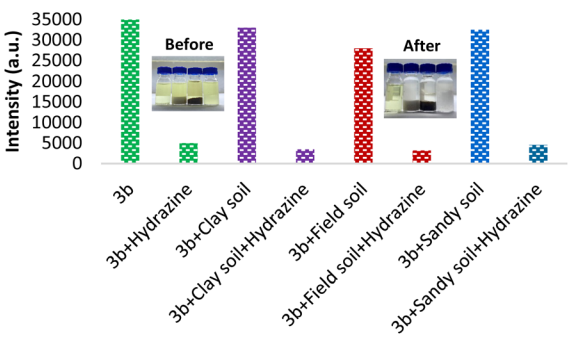

Fig. 6 Emission intensity of SBC **3b** (0.5 μM; 537 nm) after the addition of different soils in methanol with and without hydrazine.

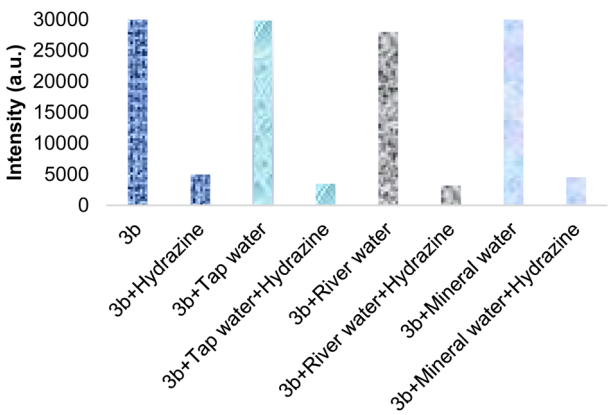

Fig. 7 Emission intensity of SBC **3b** (0.5 μM; 537 nm) after the addition of different water samples in methanol with and without hydrazine.

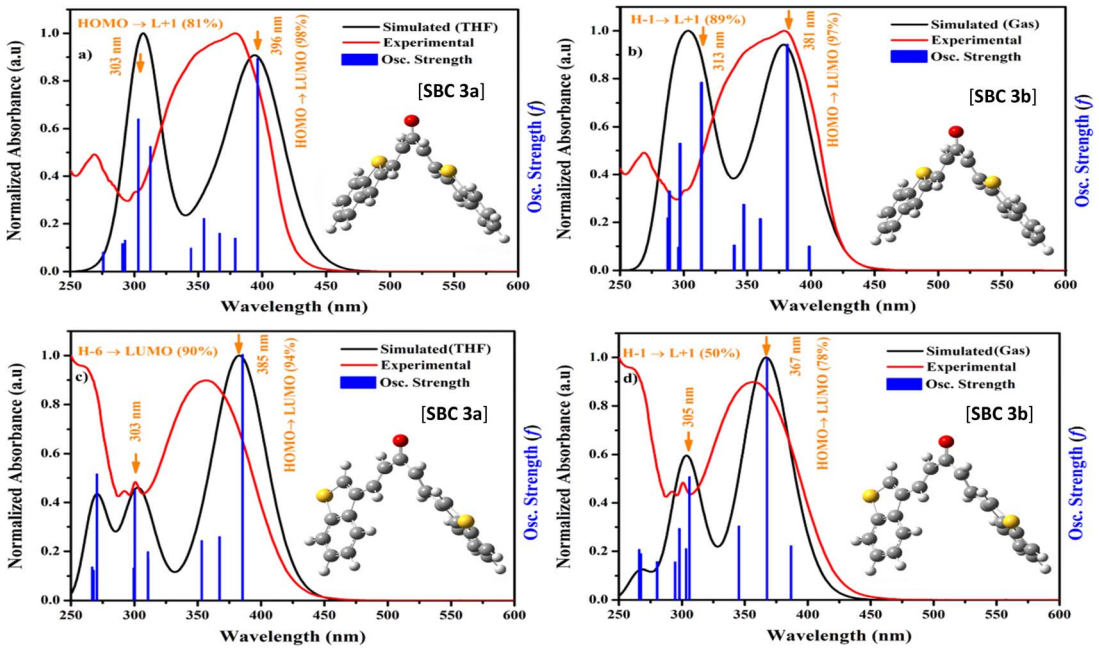

Fig. 8 Comparative study of the UV-absorption, along with its oscillation strength: (a) SBC **3a** in a solvent-simulated environment, (b) SBC **3a** in a gas-simulated environment, (c) SBC **3b** in a solvent-simulated environment, and (d) SBC **3b** in a gas-simulated environment.

Gaussian G09 with the B3LYP/6-31(G) base set was used to calculate the theoretical calculation by vertical excitation.[42–44] The optimized structures of SBC **3a** and **3b** are noted in Table S1,† and with the respective atom labelling shown in Fig. S9.† The UV-absorption study of SBC **3a** and **3b** was calculated in the gas and solvent (methanol) phase, and compared with the experimental outcomes. In addition, we compared their oscillation strength and all the relative data incorporated in Fig. 8.

SBC **3a** in the solvent shows an absorption wavelength at 396 nm with 0.67 oscillation strength, and the HOMO → LUMO contribution is 98%. In the case of the gas phase, SBC **3a** showed an absorption wavelength at 381 nm with 0.50 oscillation strength, and the HOMO → LUMO contribution is 97%. A second oscillation strength of 0.41 was found at 313 nm, and the H−1 → L+1 contribution is 89% (Table S2†). Both gas and solvent phases are matched with experimental analysis,

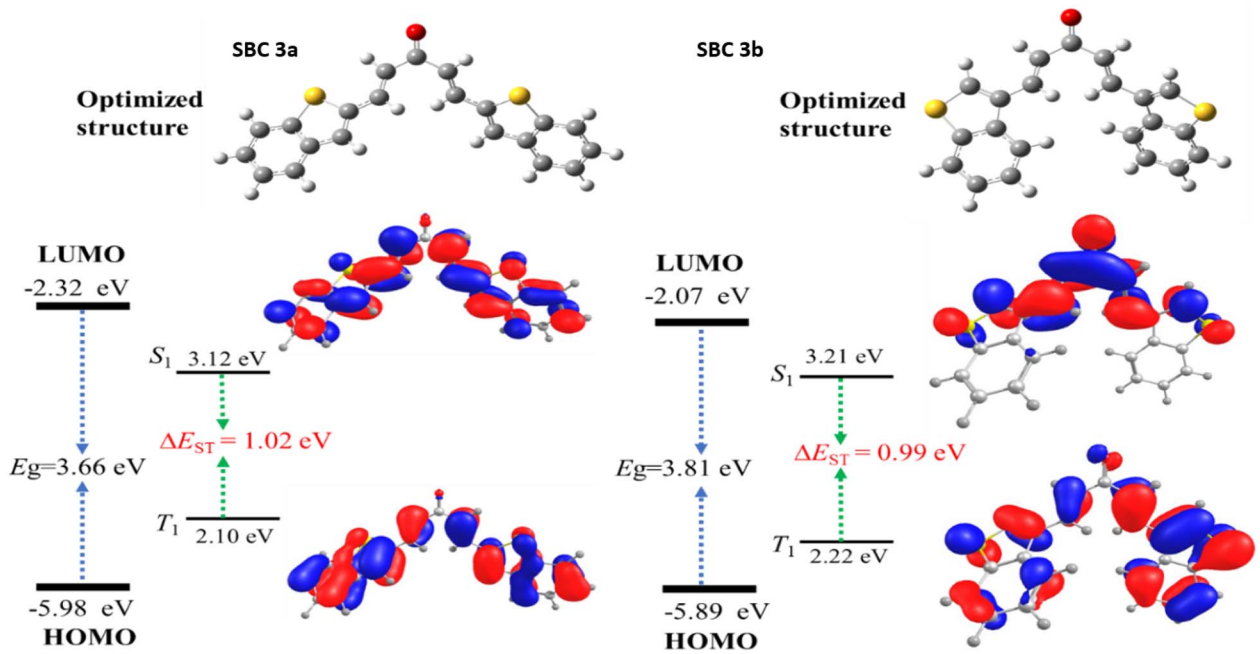

Fig. 9 Calculated HOMO and LUMO energy levels for SBC **3a** and **3b** with their frontier orbitals and their singlet–triplet excited states.

although the gas simulation is better matched, as compared with the gas and solvent phase (Fig. 8).

SBC **3b** in the solvent phase showed major oscillations at 0.39, 0.17 and 0.15 with absorption wavelengths at 385, 270 and 303 nm, and its contribution was found to be HOMO → LUMO (94%), H−6 → LUMO (90%) and H−1 → L+1 (77%), respectively. Meanwhile, the gas phase showed 367 nm absorption with 0.30 oscillation strength and a HOMO → LUMO contribution of 78%. The second highest oscillation is 0.12, and its H−1 → L+1 contribution was found to be 50% (Fig. 8c, d and Table S3†). SBC **3b** in the solvent and gas phases nearly matched with the experimental outcomes (10–20 nm variation).

In addition, the measured bond angles and their dihedral angles of SBC **3a** and **3b** are tabulated in Table S1.† The bond angle and dihedral angles of both molecules both show a similar observation at the α,β-unsaturated carbonyl group. Due to the presence of the sulphur group attachment at different 2 and 3rd positions, there is a slight variation of the 3rd-degree bond angle. Overall, the molecule represented a ''v'' shape with a similar distribution towards the right and left side of the carbonyl centre. The frontier molecular orbitals of the SBC **3a** and **3b** were calculated to find the electron distribution in the molecule, and are represented in Fig. 8 (Fig. S10,† gas phase). The HOMO and LUMO of SBC **3a** are located at −5.98 eV and −2.32 eV, respectively, and the calculated energy gap is 3.66 eV. In the case of SBC **3b**, the HOMO and LUMO are −5.89 eV and −2.07 eV, respectively, and the energy gap is 3.81 eV. As compared to SBC **3a**, **3b** exhibited a higher energy difference of HOMO–LUMO (0.15 eV), which is expected due to the presence of the sulphur-containing 5-membered ring attachment at the 3rd carbon to the α,β-unsaturated carbonyl group. The detailed HOMO–LUMO levels are represented in Table S4.† The electron distribution on HOMO of SBC **3a** is located mainly on benzo[*b*]thiophen, and LUMO is located mostly on the molecule including the carbonyl group. Meanwhile, the electron distribution of HOMO of SBC **3b** is mostly located on the conjugated portion, and the LUMO is mainly distributed on the α,β-unsaturated carbonyl group. The presence of a position change of sulphur at 2 and 3 leads to a large difference in the electron distribution. Furthermore, the presence of sulphur in SBC **3b** supressed the electrons on benzene, where the 5-membered ring is attached. The calculated singlet triplet energy levels are shown with the energy difference at approximately 1 eV, which is good for effective fluorescence emission behaviour. These outcomes indicate that the current synthesized molecules can efficiently produce fluorescence emission, which is used for the selective detection of hydrazine. Here, we have performed a basic asymptotic fraction functional (Tables S3 and S4†). However, the full range-separated functional may give better HOMO/LUMO and TDDFT energies (Fig. 9).[45–47]

4 Conclusion

A straightforward Claisen–Schmidt condensation through two comparative protocols catalyzed by KOH/pyrrolidine with benzothiophene aldehydes and acetone yielded two different hydrazine-detecting molecules. The results have proven KOH as a more effective and pyrrolidine as a more efficient catalyst for the synthesis of these semi-bis-chalcone (SBCs) scaffolds. The structures of the synthesized compounds were confirmed by NMR, IR and HRMS analyses. Generally, chalcones are photoluminescent moieties; therefore, the photophysical properties of the prepared molecules were investigated by UV-visible and fluorescence analysis in various polar and non-polar solvents. Due to intramolecular charge-transfer (ICT), the prepared SBCs exhibit high fluorescence in both solution and solid states. The obtained results of the photophysical properties and their DFT-TDDFT theoretical correlation suggest that the prepared SBCs can be optimized for their applications in optoelectronics, sensing, and bio imaging. Looking at their photoluminescent nature, the selective benzothiophene 2-carbaldehyde SBC **3a** molecule has been used for hydrazine detection with dual spectroscopies. In the presence of hydrazine, colorimetric and ratiometric fluorescence alterations for **3b** were detected because they have an activated α,β-unsaturated carbonyl group that is highly reactive towards the nucleophilic hydrazine. The detailed sensing studies of this approach includes the selectivity, anti-interference capacity (pH, organic and inorganic), limit of detection, and solvent-dependent sensing efficiency. We believe that the outcome of these sensing methods will encourage the future design of real-time probes for hydrazine and a few other chemicals with diverse applications.

Data availability

Additional data related to the main manuscript are available in the ESI.†

Author contributions

Conceptualization of the work, funding acquisition, supervision, resources, writing – original draft and review – editing were performed by Paresh. Detailed investigation, data curation, formal analysis, methodology, validation and visualization were performed by Nidhi, Dinkal, Amar and Niteen. The computational work was performed and interpreted by B. Rajamouli.

Conflicts of interest

The authors declare that they have no known competing financial interests or personal relationships that could have appeared to influence the work reported in this paper.

Acknowledgements

The authors would like to acknowledge the financial support from GSBTM, Govt. of Gujarat (File No. GSBTM/JD(R&D)/626/22-23/00018349). The authors are also thankful to Aether Industry, Ltd for mass analysis.

References

1 S. P. Nikumbh, A. Raghunadh, V. N. Murthy, R. Jinkala, S. C. Joseph, Y. L. N. Murthy, B. Prasad and M. Pal, A greener approach towards double heteroarylation of N, O and S nucleophiles: synthesis of bioactive polynuclear fused N-heteroarenes, *RSC Adv.*, 2015, **5**, 74570–74574.
2 S. Maheshwaran, W. H. Chen, S. L. Lin, M. Ghorbanie and A. T. Hoang, Electroanalytical overview: the electroanalytical sensing of hydrazine, *Environ. Sci.: Adv.*, 2024, **3**, 154–176.
3 M. Devi, P. Kumar, R. Singh, L. Narayan, A. Kumar, J. Sindhu, S. Lal, K. Hussain and D. Singh, A comprehensive review on synthesis, biological profile and photophysical studies of heterocyclic compounds derived from 2, 3-diamino-1, 4-naphthoquinone, *J. Mol. Struct.*, 2022, **1269**, 133786.
4 P. N. Patel, D. H. Desai, N. C. Patel and A. G. Deshmukh, Efficient multicomponent processes for synthesis of novel poly-nuclear hetero aryl substituted terpyridine scaffolds: Single crystal XRD study, *J. Mol. Struct.*, 2022, **1250**, 131737.
5 C. Feng, M. Lv, J. Shao, H. Wu, W. Zhou, S. Qi, C. Deng, X. Chai, H. Yang, Q. Hu and C. He, Lattice Strain Engineering of Ni2P Enables Efficient Catalytic Hydrazine Oxidation-Assisted Hydrogen Production, *Adv. Mater.*, 2023, **35**(42), 2305598.
6 S. Ma, B. Yu, B. Y. Xia and Y. Bo, A pyridinic nitrogen-rich carbon paper for hydrazine oxidation-hybrid seawater electrolysis toward efficient H2 generation, *Sci. China Mater.*, 2024, **67**, 752761.
7 T. Vyas, H. Kumar, G. Nagpurea and A. Joshi, Fiber-optic thin film chemical sensor of 2, 4 dinitro-1-chlorobenzene and carbon quantum dots for the point-of-care detection of hydrazine in water samples, *Environ. Sci.: Water Res. Technol.*, 2024, **10**, 1481–1491.
8 J. Ma, X. Kong, M. Zhao, Z. Jiao, X. Zhang, H. Xie and Z. Zhang, A water-soluble red-emitting fluorescence probe for detecting hazardous hydrazine in environmental waters and bio-systems, *Sci. Total Environ.*, 2024, **944**, 173810.
9 G. Alberti, C. Zanoni, V. Losi, L. R. Magnaghi and R. Biesuz, current trends in polymer based sensors, *Chemosensors*, 2021, **9**, 108.
10 M. F. Maitz, Applications of synthetic polymers in clinical medicine, *Biosurf. Biotribol.*, 2015, **1**(3), 161–176.
11 E. Kandemir, M. Özkütük, B. Aydınera, N. Seferoğluc, H. Erer and Z. Seferoğlu, Novel fluorescent coumarin-thiazole based sensors for selective determination of cyanide in aqueous media, *J. Mol. Struct.*, 2022, **1249**, 131593.
12 U. Krishnan, S. Manickam and S. K. Iyer, Turn-off fluorescence of imidazole-based sensor probe for mercury ions, *Sens. Diagn.*, 2024, **3**, 87–94.
13 C. Zhuang, W. Zhang, C. Sheng, W. Zhang, C. Xing and Z. Miao, Chalcone: a privileged structure in medicinal chemistry, *Chem. Rev.*, 2017, **117**(12), 7762–7810.
14 Y. Fu, D. Liu, H. Zeng, X. Ren, B. Song, D. Hu and X. Gan, New chalcone derivatives: synthesis, antiviral activity and mechanism of action, *RSC Adv.*, 2020, **10**, 24483–24490.
15 P. N. Patel, K. D. Patel and H. S. Patel, Synthesis and biological study of novel 5-{(4-(6, 7-dihydrothieno-[3, 2-*c*] pyridin-5 (4H)-ylsulfonyl) phenylamino)-methyl} quinolin-8-ol and its metal complexes, *Chin. Chem. Lett.*, 2011, **22**(11), 1297–1300.
16 W. Sijia, W. Enting and Y. Yuan, Detection of furan levels in select Chinese foods by solid phase microextraction-gas chromatography/mass spectrometry method and dietary exposure estimation of furan in the Chinese population, *Food Chem. Toxicol.*, 2014, **64**, 34–40.
17 A. Torbica, D. Horvat, D. Zivancev, M. Belović, G. Šimić, D. Magdić, N. Đukić and K. Dvojković, Prediction of the genetic similarity of wheat and wheat quality by reversed-phase high-performance liquid chromatography and lab-on-chip methods, *Acta Aliment.*, 2017, **46**, 137–144.
18 S. Seidi and L. Alavi, Novel and rapid deep eutectic solvent (DES) homogeneous liquid-liquid Microextraction (HLLME) with flame atomic absorption spectrometry (FAAS) detection for the determination of copper in vegetables, *Anal. Lett.*, 2019, **52**, 2092–2106.
19 X. Luo and L. T. Lim, Curcumin-loaded electrospun nonwoven as a colorimetric indicator for volatile amines, *LWT–Food Sci. Technol.*, 2020, **128**, 109493.
20 A. M. Razdari, M. G. Varnamkhasti, Z. Izadi, S. Rostami, A. A. Ensafi, M. Siadat and E. Losson, Detection of sulfadimethoxine in meat samples using a novel electrochemical biosensor as a rapid analysis method, *J. Food Compos. Anal.*, 2019, **82**, 103252.
21 B. Mohan, N. M. Kunhumon and S. Shanmugaraju, Fluorescence sensing and bioimaging of Cu (II) ions using amino-1, 8-naphthalimide-based small-molecule chemosensors, *Sens. Diagn.*, 2023, **2**, 11581175.
22 S. Singh, N. Kumari, B. K. Kanungo and M. Baral, Hydroxypyridinone based chelators: a molecular tool for fluorescence sensing and sensitization, *Sens. Diagn.*, 2024, **3**, 968986.
23 L. Liu, M. Xing, Y. Han, X. Zhang, P. Li, D. Cao, S. Zhao, L. Ma and Z. Liu, Sensing for hydrazine of a pyrene chalcone derivative with acryloyl terminal group, *Spectrochim. Acta, Part A*, 2022, **264**, 120272.
24 L. Yan, S. Zhang, Y. Xie, X. Mu and J. Zhu, Recent progress in the development of fluorescent probes for the detection of hydrazine, *Crit. Rev. Anal. Chem.*, 2022, **52**, 210–229.
25 B. Shi, Y. Chai, P. Qin, X. X. Zhao, W. Li, Y. M. Zhang, T. B. Wei, Q. Lin, H. Yao and W. J. Qu, Detection of aliphatic aldehydes by a pillar[5]arene-based fluorescent supramolecular polymer with vaporchromic behavior, *Chem.–Asian J.*, 2022, **17**, e202101421.
26 H. Xing, Y. Yu, J. Liu, P. Qin, J. W. Y. Lam, B. Shi, G. Xie and B. Z. Tang, A Discrete platinum(II) metallacycle harvesting triplet excitons for solution-processed deep-red organic light-emitting diodes, *Adv. Opt. Mater.*, 2022, **10**, 2101925.
27 E. N. Okolo, D. I. Ugwu, B. E. Ezema, J. C. Ndefo, F. U. Eze, C. G. Ezema, J. A. Ezugwu and O. T. Ujam, New chalcone derivatives as potential antimicrobial and antioxidant agent, *Sci. Rep.*, 2021, **11**, 21781.

28 P. N. Patel and A. Chadha Synthesis, single crystal structure and spectroscopic aspects of Benzo [b] thiophene-3-carbaldehyde based chalcones, *J. Chem. Crystallogr.*, 2016, **46**, 245–251.
29 S. Tandel, N. C. Patel, S. Kanvah and P. N. Patel, An efficient protocol for the synthesis of novel hetero-aryl chalcone: A versatile synthon for several heterocyclic scaffolds and sensors, *J. Mol. Struct.*, 2022, **1269**, 133808.
30 S. N. Tandel, A. G. Deshmukh, B. U. Rana and P. N. Patel, Studies of novel benzofuran based chalcone scaffolds: A dual spectroscopic approach as selective hydrazine sensor, *Chem. Phys. Lett.*, 2023, **817**, 140426.
31 S. Halder, B. Nayak, B. Bhattacharjee, A. Ramesh and G. Das, Insight into the aggregation prospective of Schiff base AIE gens enabling an efficient hydrazine sensor in their aggregated state, *J. Mater. Chem. C*, 2021, **9**, 8596–8605.
32 Y. Jung, I. G. Ju, Y. H. Choe, Y. Kim, S. Park, Y. M. Hyun, M. S. Oh and D. Kim, Hydrazine exposé: the next-generation fluorescent probe, *ACS Sens.*, 2019, **4**, 441–449.
33 X. Y. Zhang, Y. S. Yang, W. Wang, Q. C. Jiao and H. L. Zhu, Fluorescent sensors for the detection of hydrazine in environmental and biological systems: Recent advances and future prospects, *Coord. Chem. Rev.*, 2020, **417**, 213367.
34 Y. Zhang, Z. Wang, J. Song, M. Li, Y. Yang, X. Xu, H. Xu and S. Wang, A simple camphor based AIE fluorescent probe for highly specific and sensitive detection of hydrazine and its application in living cells, *Anal. Methods*, 2019, **11**, 3958–3965.
35 G. Wu, X. Tang, W. Ji, K. Lai and Q. Tong, A turn-on fluorescent probe based on coumarin-anhydride for highly sensitive detection of hydrazine in the aqueous solution and gas states, *Methods Appl. Fluoresc.*, 2017, **5**(1), 015001.
36 R. Maji, A. K. Mahapatra, K. Maiti, S. Mondal, S. S. Ali, P. Sahoo, S. Mandal, M. R. Uddin, S. Goswami, C. K. Quah and H. K. Fun, A highly sensitive fluorescent probe for detection of hydrazine in gas and solution phases based on the Gabriel mechanism and its bioimaging, *RSC Adv.*, 2016, **6**, 70855–70862.
37 W. Chen, W. Liu, X. J. Liu, Y. Q. Kuang, R. Q. Yu and J. H. Jiang, A novel fluorescent probe for sensitive detection and imaging of hydrazine in living cells, *Talanta*, 2017, **162**, 225–231.
38 Q. Fang, L. Yang, H. Xiong, S. Han, Y. Zhang, J. Wang, W. Chen and X. Song, Coumarinocoumarin-based fluorescent probe for the sensitive and selective detection of hydrazine in living cells and zebra fish, *Chin. Chem. Lett.*, 2020, **31**, 129–132.
39 W. Zhang, F. Huo, T. Liu and C. Yin, Ratiometric fluorescence probe for hydrazine vapor detection and biological imaging, *J. Mater. Chem. B*, 2018, **6**, 8085–8089.
40 X. Jin, C. Liu, X. Wang, H. Huang, X. Zhang and H. Zhu, A flavone-based ESIPT fluorescent sensor for detection of N_2H_4 in aqueous solution and gas state and its imaging in living cells, *Sens. Actuators, B*, 2015, **216**, 141–149.
41 S. N. Tandel, P. Mistry and P. N. Patel, Novel chalcone scaffolds of benzothiophene as an efficient real time hydrazine sensor: Synthesis and single crystal XRD studies, *J. Mol. Struct.*, 2023, **1274**, 134495.
42 L. Zhu, L. Du, G. Caoa and Z. Cai, AI-guided electro-decomposition of persistent organic pollutants: a long-awaited vision becoming reality?, *Environ. Sci.: Adv.*, 2023, **2**, 1302–1305.
43 G. R. Jenness and M. K. Shukla, What can Blyholder teach us about PFAS degradation on metal surfaces?, *Environ. Sci.: Adv.*, 2024, **3**, 383–401.
44 M. Fischer, Density functional theory study of hydrophobic zeolites for the removal of triclosan from aqueous solution, *Environ. Sci.: Adv.*, 2023, **2**, 1082–1098.
45 M. E. Foster and B. M. Wong, Nonempirically Tuned Range-Separated DFT Accurately Predicts Both Fundamental and Excitation Gaps in DNA and RNA Nucleobases, *J. Chem. Theory Comput.*, 2012, **8**, 2682–2687.
46 B. M. Wong and T. H. Hsieh, Optoelectronic and Excitonic Properties of Oligoacenes: Substantial Improvements from Range-Separated Time-Dependent Density Functional Theory, *J. Chem. Theory Comput.*, 2010, **6**, 3704–3712.
47 B. M. Wong, M. Piacenzab and F. D. Sala, Absorption and fluorescence properties of oligothiophene biomarkers from long-range-corrected time-dependent density functional theory, *Phys. Chem. Chem. Phys.*, 2009, **11**, 4498–4508.